05HQGR0064

COLLABORATIVE RESEARCH (USC AND UMASS): MECHANICAL MODELS OF THREE-DIMENSIONAL ACTIVE FAULTING IN THE VENTURA BASIN

Michele Cooke
University of Massachusetts
611 North Pleasant Street
Amherst, MA
01003-9297
Voice: 413-577-3142
FAX: 413-545-1200
cooke@geo.umass.edu

Susan Owen
University of Southern California
3651 Trousdale Parkway
Los Angeles, CA
90089-0740
Voice: 213 740-6308
FAX: 213 740-8801
owen@usc.edu

ELEMENT III. Research on earthquake occurrence, physics and effects

Research supported by the U.S. Geological Survey (USGS), Department of the Interior, under USGS award number (Recipient, insert award number). The views and conclusions contained in this document are those of the authors and should not be interpreted as necessarily representing the official policies, either expressed or implied, of the U.S. Government.

1. Introduction

Ventura basin is one of the most tectonically active basins in southern California with 7 ± 2 mm/yr of GPS measured regional shortening across the basin [*Donnellan, et al.*, 1993]. The 1994 M 6.7 Northridge earthquake ruptured along one of the Ventura basin fault systems, took the lives of 60 people and caused $15 billion in property damage. While the Ventura basin has significant agricultural land use, and much of the basin is relatively rural, the proximity of the active faults of the Ventura basin to large urban areas (e.g. Los Angeles and the San Fernando Valley), exposes these areas to substantial seismic risk. With the growth of small towns in the basin, and the subsequent addition of new housing communities, in particular the 22,000 unit Newhall Ranch development, comes increased vulnerability to seismic hazards. Understanding of the behavior and interaction of the faults in the Ventura basin will help refine the Probabilistic Seismic Hazard Assessment (PSHA) in the region, and help in lowering losses caused by future earthquake events on these faults.

Mitigation of future earthquake damage relies on accurate assessment of fault configuration, slip rates, and seismogenic area. These are required by predictive earthquake algorithms used to calculate strong ground motion. Paleoseismologic observations and kinematic folding studies have constrained slip rates along some exposed or near surface faults within the Ventura basin [e.g. *Azor, et al.*, 2002; *Cemen*, 1979; *Dolan and Rockwell*, 2001; *Huftile and Yeats*, 1995; *Rockwell*, 1988; *Yeats*, 1988], however these data cannot fully constrain the configuration and activity level of all subsurface faults. Additional data is needed in order to help constrain the three-dimensional fault configuration and slip rates. This study constructs three-dimensional mechanical models of the Ventura Basin faults in order to constrain proposed fault configurations and slip rates. The slip rates results from the mechanical models can be compared to available geologic rates. By enhancing the models so that they produce interseismic strain at the surface, the results can also be compared to geodetic data. We are fortunate to have data from the Southern California Integrated Geodetic Network (SCIGN) available for this purpose.

The validity of the model comparison depends on starting with the most accurate rates of surface deformation. Since the installation of SCIGN, scientists have recognized that pumping and recharge of fluids such as oil and groundwater can contribute significantly to the geodetically measured ground deformation [e.g. *Bawden, et al.*, 2001]. We have begun working on removing this component of the geodetic signal as reliably as possible in order to acquire the most accurate measurements of ground deformation caused purely by fault-related interseismic strain accumulation. Continuous GPS provides the temporal resolution to address the issue of seasonal or fluid-related deformation. We will use SCIGN GPS time series data and available information on rainfall, groundwater pumping, and oil pumping in order to best characterize and then remove the non-tectonic signal from the geodetic data. This allows us to use the most accurate geodetic estimates of tectonic deformation for comparison to three-dimensional mechanical fault models. Although we explored using InSAR for improved spatial resolution of the tectonic deformation, available InSAR

scenes did not provide adequate coherence and purchasing additional scenes was prohibitively expensive.

Geodetic rates of tectonic surface deformation are believed to result from continuous and long-term deformation below the seismogenic crust. *Donnellan et al*. [1993] first estimated fault locking depths and fault slip rates in the Ventura basin using results from campaign GPS data. The low convergence rates compared to geologic estimates and the anomalously shallow fault locking depths required to fit the steep deformation gradients across the basin prompted researchers to test models that included a viscoelastic lower crust and upper mantle as well as a compliant basin [*Hager, et al.*, 1999]. These two-dimensional models were successful in resolving the convergence rate and locking depth discrepancies. The models, however, required simplifications of the basin fault geometry.

We use three-dimensional Boundary Element Method (BEM) models, which permits investigation of complex, non-planar and intersecting active fault surfaces such as within the Ventura basin (Fig. 1). To determine the sensitivity of interseismic surface velocities to complex fault geometry, we compare the results of a geologically representative model to a model with planar fault surfaces. Although planar faults or two-dimensional models may adequately approximate faulting in some regions, without explicit investigation of fault irregularities the errors accrued by such assumptions are uncertain. While we will ignore the viscoelastic nature of the lower crust, we have developed a model that includes a compliant basin. Geologic slip rates predicted by the model can also be directly compared to paleoseismic and geologically inferred rates within the last ~10,000 years. Estimates of geologic slip rates on the basin faults are determined for both geologically representative and planar fault models and compared to independently determined geologic fault slip rates. Because the mechanical models calculate slip rate vectors at all points on the fault surfaces, these results can be used to extrapolate slip rates from locations of known geologic rates, such as determined from trench data. These slip rate distributions can also be used to estimate seismic hazard along poorly constrained faults and guide location of future paleoseismic investigations.

2. Methods

2.1 GPS time series analysis

In order to isolate the surface deformation due to strain accumulation on the Ventura basin faults, we must first subtract the effects of strain accumulation on San Andreas fault from the GPS data. This process is relatively straightforward as other studies have determined the slip rates and locking depths for the San Andreas fault. We use dislocations in a homogeneous elastic half-space [Okada, 1985] calculate the relatively simple-geometried San Andreas interseismic surface deformation.

Geodetic signals are sensitive to more than just tectonic ground motion. Continuous stations within the SCIGN network, especially where installed on young bedrock or in sedimentary basins, are prone to strong seasonal and annual signals (Figure 2). The Ventura basin is a relatively large agricultural region, dominated by citrus production. The area is extensively irrigated, with significant ground-water withdrawal. Seasonal precipitation in the region supplies the majority of the shallow ground-water recharge. Pumping and injection of groundwater in the region can have

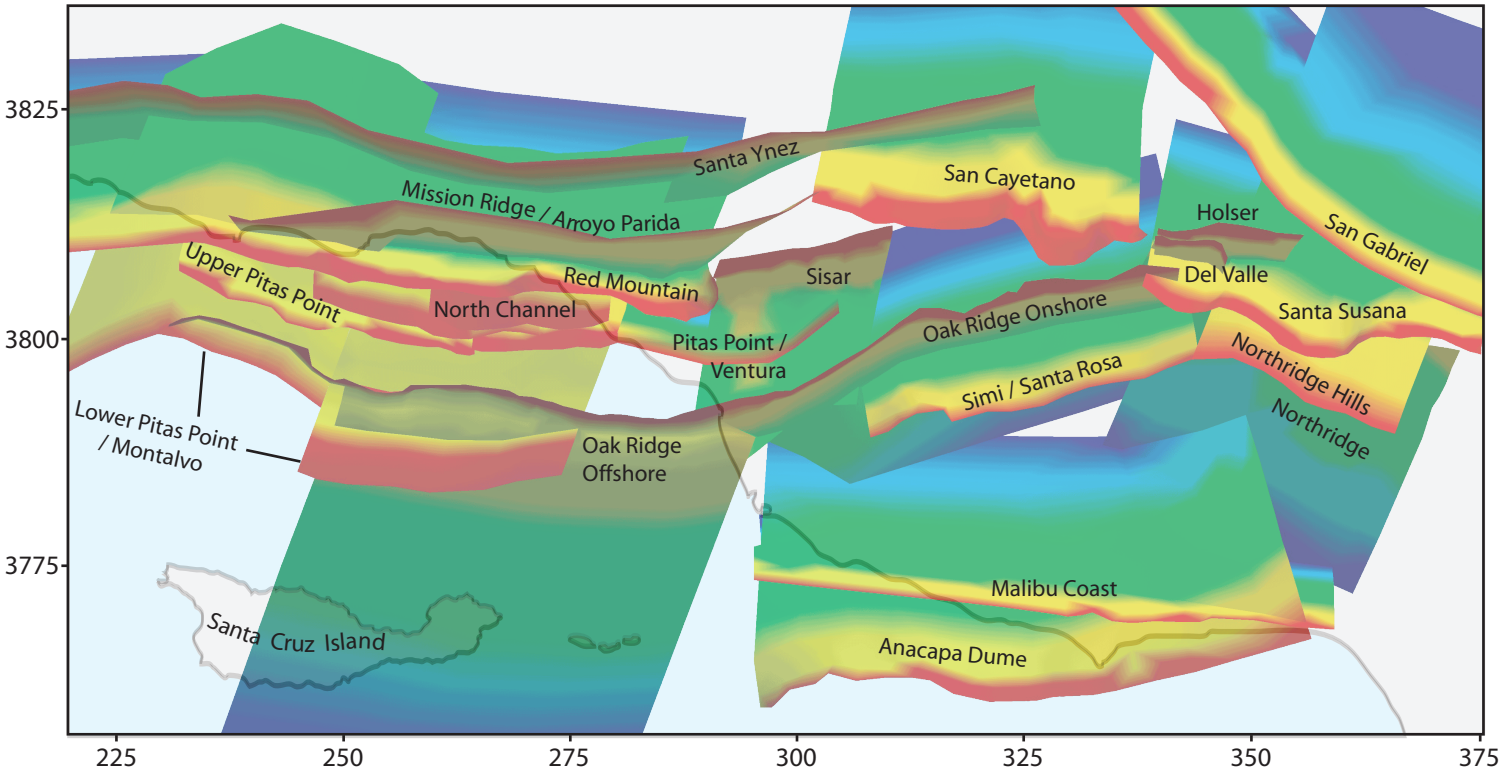

Figure 1 – Map view of the 3-dimensional fault surfaces used in the topology model in this study. The upper surfaces are defined in the community fault model version 2.5 and are extended to 27.5 km as shown in figure 2. Red is the surface of the Earth and dark blue is 27.5 km depth. South-dipping faults are backlit to enhance differences in dip direction. Modeled surfaces are tessellated into triangular elements. Projection is UTM (NAD1927) and easting and northing are given in km.

OVLS Residuals, before and after filtering

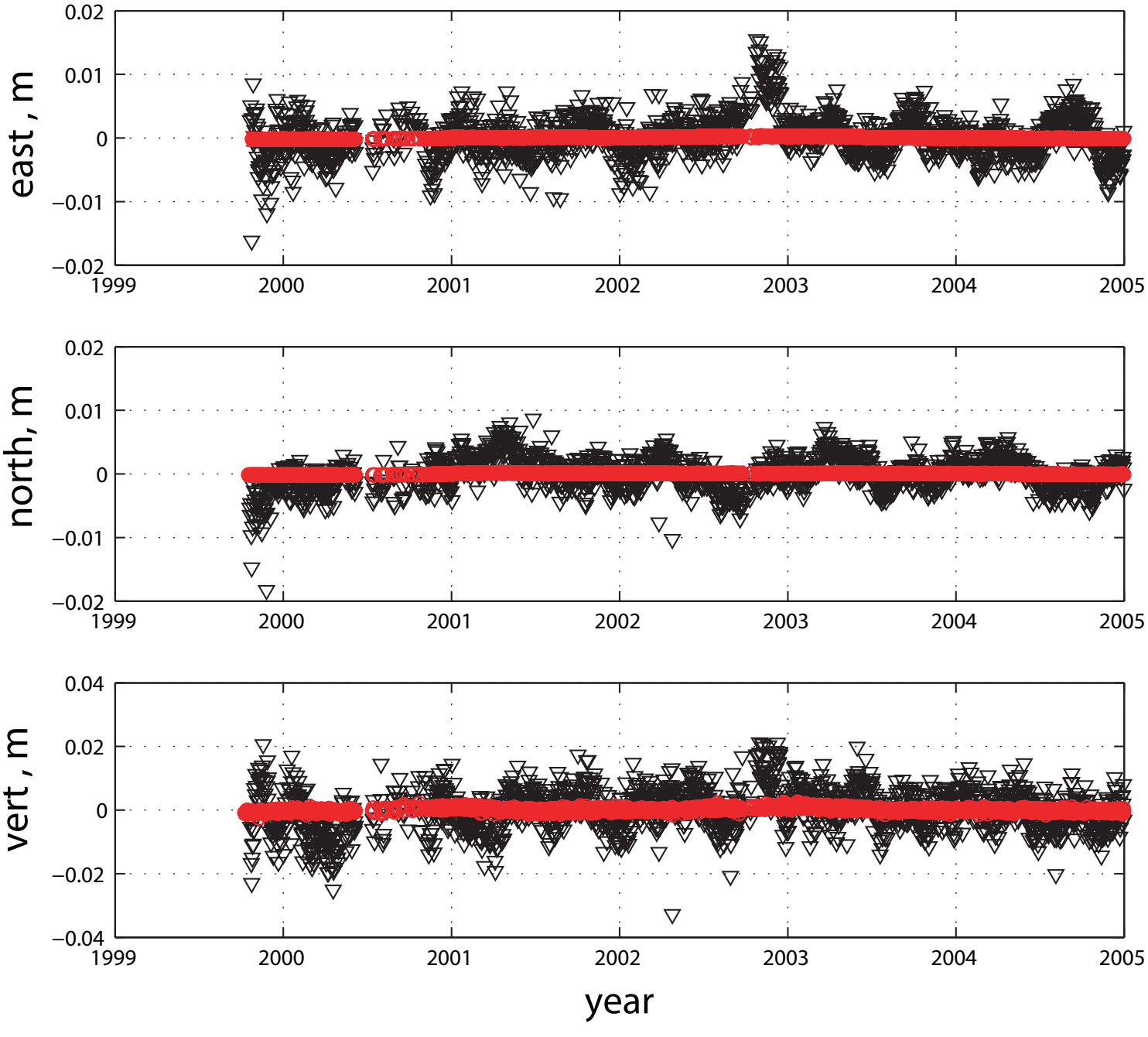

Left: In order to get the best estimate of tectonic deformation rates, we assume that the rates are linear and attempt to filter out non-linear components of time series. We first take the solutions from JPL and SOPAC and apply a common mode bias filter to the 15 sites in our region of interest. This should remove noise that is spatially correlated across the network. We then use principle component analysis to filter out the the spatially uncorrelated noise. We assume that only the linear rates of deformation are spatially and temporally correlated across the network, and we find this is true at the few mm-level. The figure to the right shows the residuals from linear fit to the original GPS solutions in black, and the residuals from the final filtered results in red. The twice filtered time series is not completely linear, but the rms of the residuals has been significantly reduced from the initial time series.

strong effects on the observed geodetic signal, consequently degrading the accuracy of the geodetically determined interseismic deformation rates.

We have analyzed the data from a subset of 16 stations within the SCIGN network in and around the Ventura basin region so as to remove annual and seasonal non-tectonic signals. In order to avoid the redundancy of reprocessing the initial network data, we are using the unfiltered time-series products available from both SCIGN processing centers, JPL and SOPAC. The position estimates from the SCIGN network data from the two processing centers have been shown to be in good agreement. The time series from 16 stations in Ventura basin region have been reviewed to carefully remove spurious outliers, offsets caused by equipment changes at continuous sites, and any corrupted data from failed or failing equipment. We then remove the common mode bias [Wdowinski et al., 1997] and the time series is rotated into a locally determined reference frame.

To remove the groundwater or atmospheric signals in the time series, which often vary seasonally we use a principal component analysis (PCA) approach [e.g., Savage and Thatcher, 1992, Savage, 1995, Aoki and Scholz, 2003], which identifies the primary temporal modes of the signal. This method is useful for resolving simultaneously observed data into a superposition of several orthogonal common modes and we have been testing its usefulness for removing non-tectonic signals from GPS time series [Austin and Owen, abs, 2004]. Another method for removing seasonal signals is to remove the best-fit sinusoid to the time series. The PCA has the advantage of not requiring a priori that the non-tectonic motion is sinusoidal in form. We have run tests on postseismic GPS data around the Hector Mine earthquake and also on synthetic time series where we could test how well we can recover the long-term velocity (i.e. tectonic motion) from the synthetic time series when we add noise and seasonal signals. We have found that the PCA is most effective at separating the tectonic and seasonal components when the seasonal signals are slightly offset in time at the different sites.

We have applied the PCA analysis to the Ventura continuous GPS data (Figure 2). This analysis requires that the data be sampled simultaneously; therefore, after testing several interpolation methods, we have used a nearest neighbor interpolation in order to fill gaps that may occur in the time series. Stations in this region have a large variation in the date of installation, and one station in particular, MUSD, was removed for school construction. In order to minimize the amount of extrapolation at the ends of the time-series, we have done our preliminary analysis on data between 23 Dec. 2000, and 13 June 2003. This time period brackets the installation of new stations at the end of 2000 and the removal of MUSD. In this case the PCA resolves into 16 different modes. The vertical signal at the 16 SCIGN stations can be almost completely accounted in a combination of the first 7 modes. Combinations of the dominant principal components can then be used to recalculate the time-series at each location. The first component is almost completely linear and accounts for approximately 80% of the long-term velocity at the stations. The subsequent modes are dominated by annual/seasonal cycles with some residual slope. Velocities calculated from the PCA filtered time series are shown in figure 3. We calculated the velocity errors so that the reduced chi-squared from the weighted least squares velocity estimate is 1. Note that with reduced scatter in the time series the errors in the velocity estimates are also lower.

Figure 3a

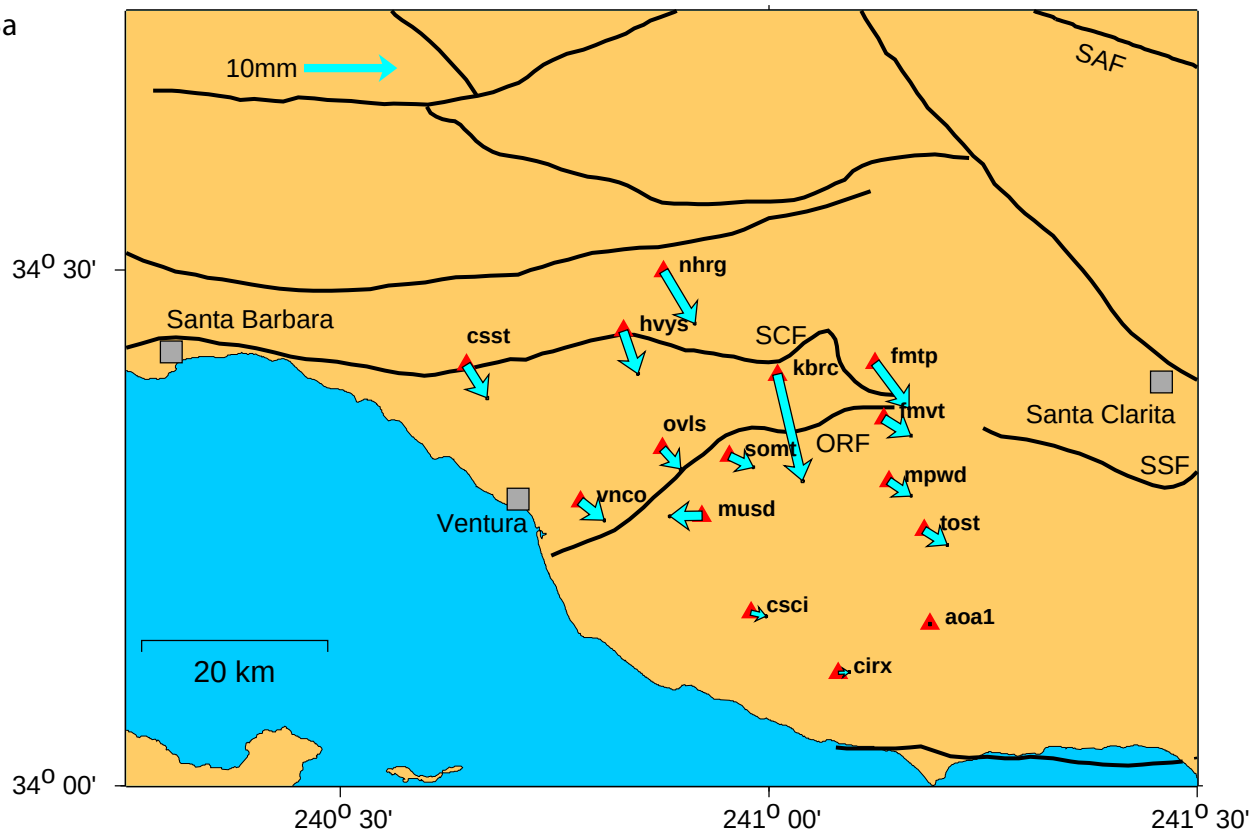

Figure 3b

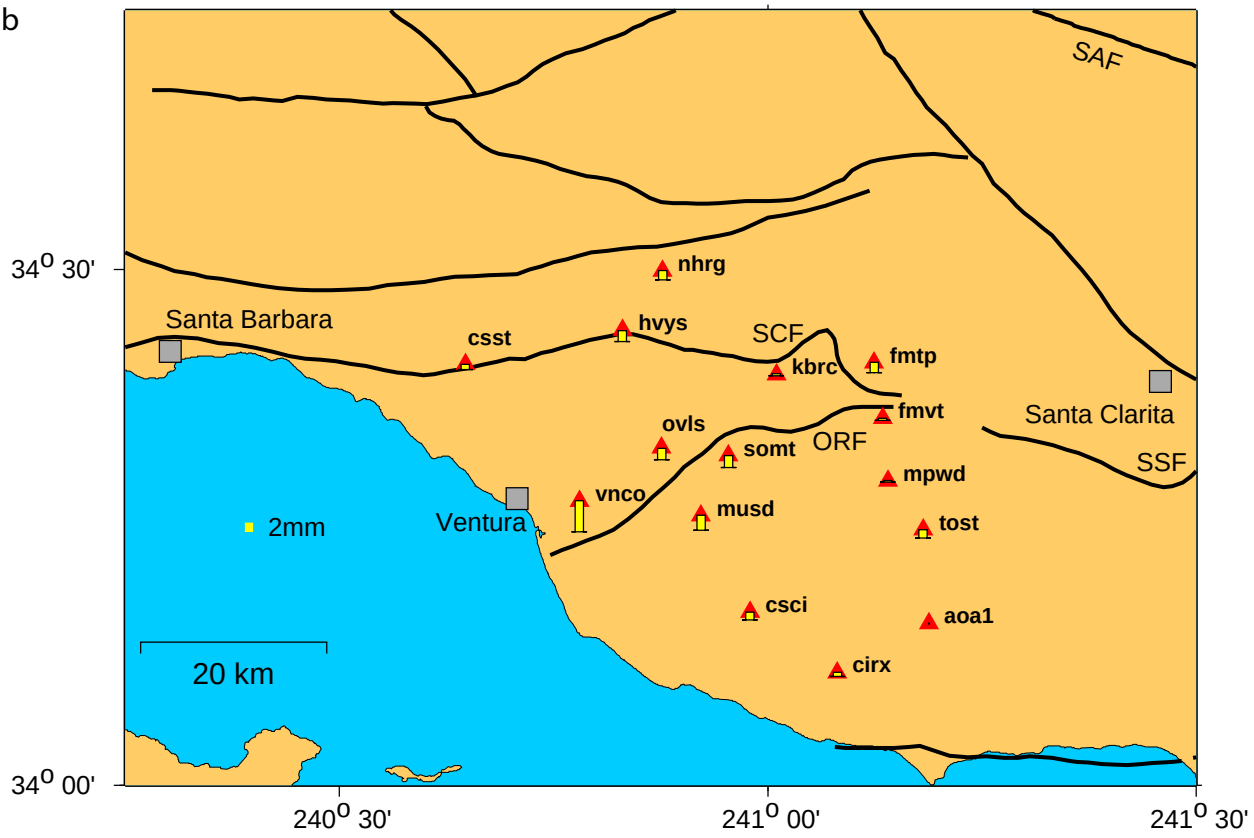

Table 1 shows the rms of the residuals, averaged over the 15 Ventura region sites, for the three different stages of filtering. The common mode bias filtering provides the greatest reduction in residual rms for this small regional network. The PCA filter decreases the rms of the vertical residuals to below 1 mm.

The results of the GPS time series analysis show general north-south tectonic convergence across the basin (Fig. 3). Large velocity gradients occur across the axis of the Ventura basin. Principal strain analysis of all the stations gives 121 nanostrain per year principal contraction at 171˚ and 36 nanostrain per year principal extension at 081˚. The MUSD station shows significant deviation from the general strain pattern, which may be related to either station integrity or localized strain due to strike slip along nearby faults.

2.2 Boundary Element Method analysis

Detailed surfaces for active faults in Southern California have been compiled within the Southern California Earthquake Center's (SCEC) Community Fault Model (CFM) [*Plesch, et al.*, 2002]. Faults of this dataset are defined at the highest resolution available from geologic maps, wells and seismic reflection data. The CFM reveals the complex intersection of faults in the Ventura region (Fig. 1).

To preserve the non-planar and complex topology of the tessellated CFM fault surfaces, we use a triangular element formulation of the Boundary Element Method implemented in POLY3D [*Thomas*, 1994]. POLY3D has been used to simulate the three-dimensional active tectonics of the Marmara Sea [*Muller and Aydin*, 2005] the Hector Mine earthquake [*Maerten, et al.*, 2005] and the Los Angeles basin [*Griffith and Cooke*, 2004; 2005; *Olson and Cooke*, 2005].

Three-dimensional interseismic models are developed in two steps (Fig. 4), first we model the geologic deformation (coseismic + interseismic) and then fault slip from that geologic model is prescribed as sub-seismogenic crustal creep along faults within the interseismic model. In the first step, remote strain is applied to simulate the tectonic deformation of the region. For the Ventura basin we applied remote strain determined from the principal strain analysis of the PCA-processed SCIGN station velocities. Because geologic deformation observed at the Earth's surface is the sum effect of coseismic slip of faults within the seismogenic crust and any aseismic fault slip or viscous flow of material below the brittle-ductile transition, we extend the fault surfaces, which in the CFM are only defined to 18 km depth, to a horizontal freely-slipping crack at 27.5 km [*Cooke, et al.*, in preparation]. This crack sits at the inferred depth of the Moho imaged in LARSE I [*Fuis, et al.*, 2001] and serves to decouple the overlying deformation so that fault slip is not resisted by the half-space formulation of the BEM models. In the geologic model, the entire fault surfaces are free to slip and interact under the remotely applied tectonic loading. Unlike interseismic models that prescribe geologic slip rates along faults, we develop a geologic model to determine fault slip distributions that are compatible with regional tectonic deformation. During interseismic periods, movements recorded at the Earth's surface reflect primarily deformation below the seismogenic crust and faults are generally locked within the seismogenic crust [e.g. *Savage and Burford*, 1970]. To simulate this interseismic deformation, fault slip from the geologic model is mapped onto the fault below the seismogenic locking depth; slip above the locking depth is zero. In essence, the interseismic modeling approach

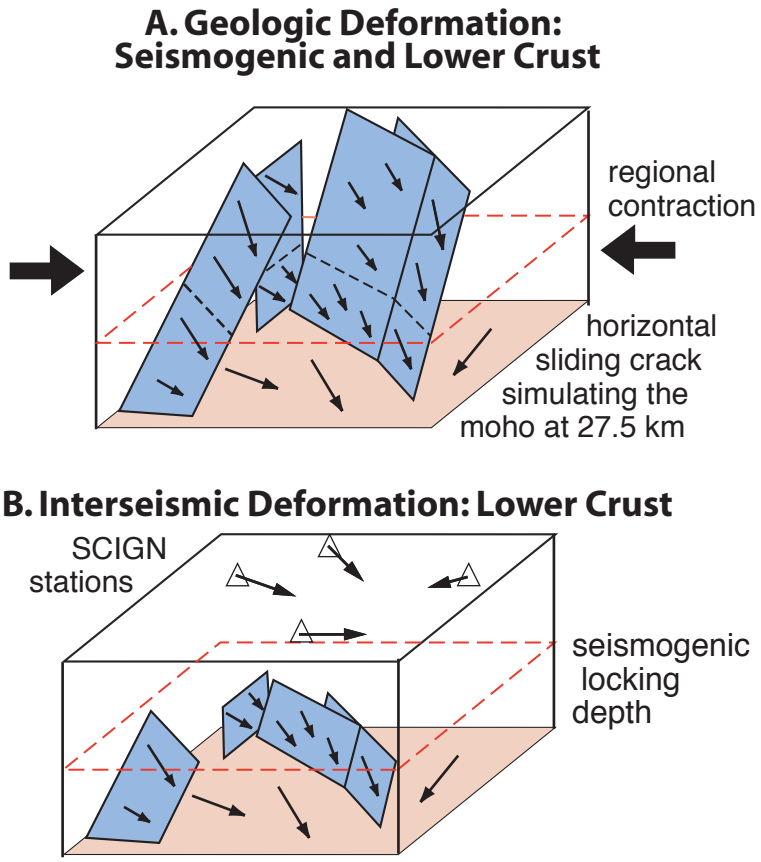

Figure 4: Two-step methodology for interseismic modeling. A) Fault surfaces within the seismogenic and lower crust to 27.5 depth freely slip under tectonic contraction and interact with each other and with a horizontal crack at 27.5 depth that represents the moho (light grey plane). The horizontal crack extends laterally far from the model to minimize edge effects within the study area. All major faults are cross-cutting at depth though some minor faults abut against major structures. This model produces slip rates that can be compared to geologic observations. B) The interseismic model is built by locking the faults above the seismogenic locking depth (dashed line) and prescribing slip below this depth to be the same as the results from the first geologic model. The surface velocities from the model can be compared to that of the SCIGN network (shown schematically with triangles).

extends from the creeping dislocation model established by *Savage and Burford* (1970) for interseismic analyses of strike-slip faults and the models of *Shen et al.* (1996) for a single thrust fault intersecting strike slip faults. However, extension of all faults within the CFM, which contains multiple thrust faults, to infinite depth gives rise to many problematic intersections. Instead we extend most the faults (several minor faults abut major faults) to a slipping detachment at 27.5 km depth in order to simulate lower crustal deformation. This detachment is deeper than that used by *Shen et al.* (1996) and provides close match to surface deformation associated with semi-infinite fault [*Cooke, et al.*, in preparation].

The rapid accumulation of sediments within the Ventura basin has produced a deep trough of relatively soft strata bounded by rigid basement highs across the basin bounding faults [e.g. *Huftile and Yeats*, 1994]. The contrasting rheology of the basin and bounding basement rocks may contribute to the deformation pattern. Because our models do not yet include compliant basin fill material within the Ventura basin, to match the geodetic convergence rates requires a shallow 5 km seismogenic locking depth. The occurrence of earthquakes to depths of >15 km in the region suggests that natural limit of aseismic creep is much deeper than 5 km. The inclusion of a compliant sedimentary material within the Ventura basin may allow for higher rates of surface contraction with deeper locking depth [*Hager, et al.*, 1999]. Future models should explore deeper locking depth with a compliant basin fill.

2.2.1 Methodology for simulating compliant basin fill

Although Poly3d does not explicitly consider heterogeneous material properties, a compliant region can be simulated by implementing an array of small, randomly oriented cracks [e.g. *Budiansky and O'Connell*, 1974]. Preliminary analysis of arrays of random cracks show that compliance increases within increasing crack spacing, crack length and with increasing applied load (Fig. 5a). Thus, choosing the appropriate crack spacing and length can approximate the desired basin compliance, relative to basement rocks, under a specific load. Within our models, the basin regions are populated with an array of randomly oriented cracks with the desired spacing and length (Fig. 5b). In future work, models with and without a compliant basin can be compared to assess the role of basin compliance on geologic slip and uplift rates and on interseismic surface velocity pattern. We expect that the homogeneous models may overestimate fault slip rate compared to geologic observations whereas a compliant basin will accommodate some of the regional contraction, reducing slip along neighboring faults.

3. Ground Surface Velocities

3.1 Comparison of interseismic model results with GPS velocities

The interseismic model of the Ventura basin with 5 km locking depth closely matches the direction and magnitude of tectonic velocities of most of the SCIGN stations within the basin (Fig. 6). Specifically, model velocities outside of the Ventura basin match station velocities better than stations within and on the edges of the basin.

Directional discrepancies are largest for stations MUSD, OVLS and SONT, which are near to one another. These discrepancies may in part reflect inaccurate

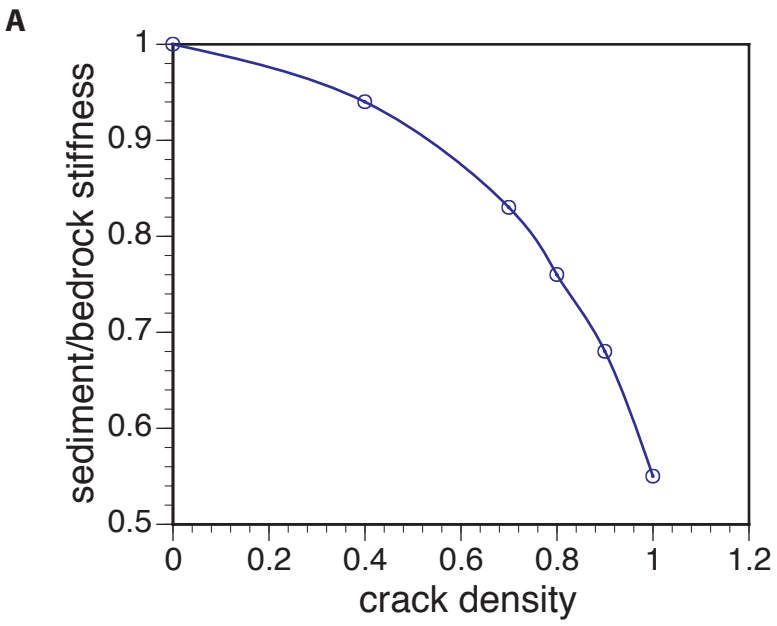

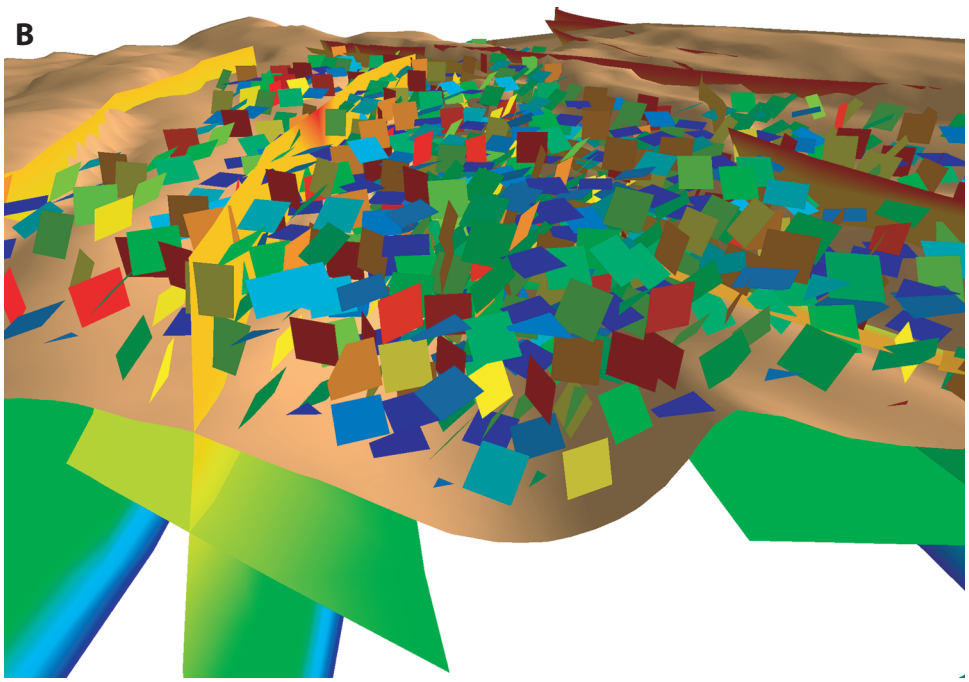

Figure 5: A) effective compliance resulting from different density (half-length/spacing) of randomly oriented cracks under stress conditions occuring within southern California. The basin has a stiffness of about 60% of the basement rock (Hager et al 1999), which can be acheived with a crack spacing just over the half-length of the crack. B) oblique view of the Los Angeles model with the sedimentary basin populated with randomly oreintated cracks. The copper surface is teh top of basement. The hue of each square crack shows the dip of that crack.

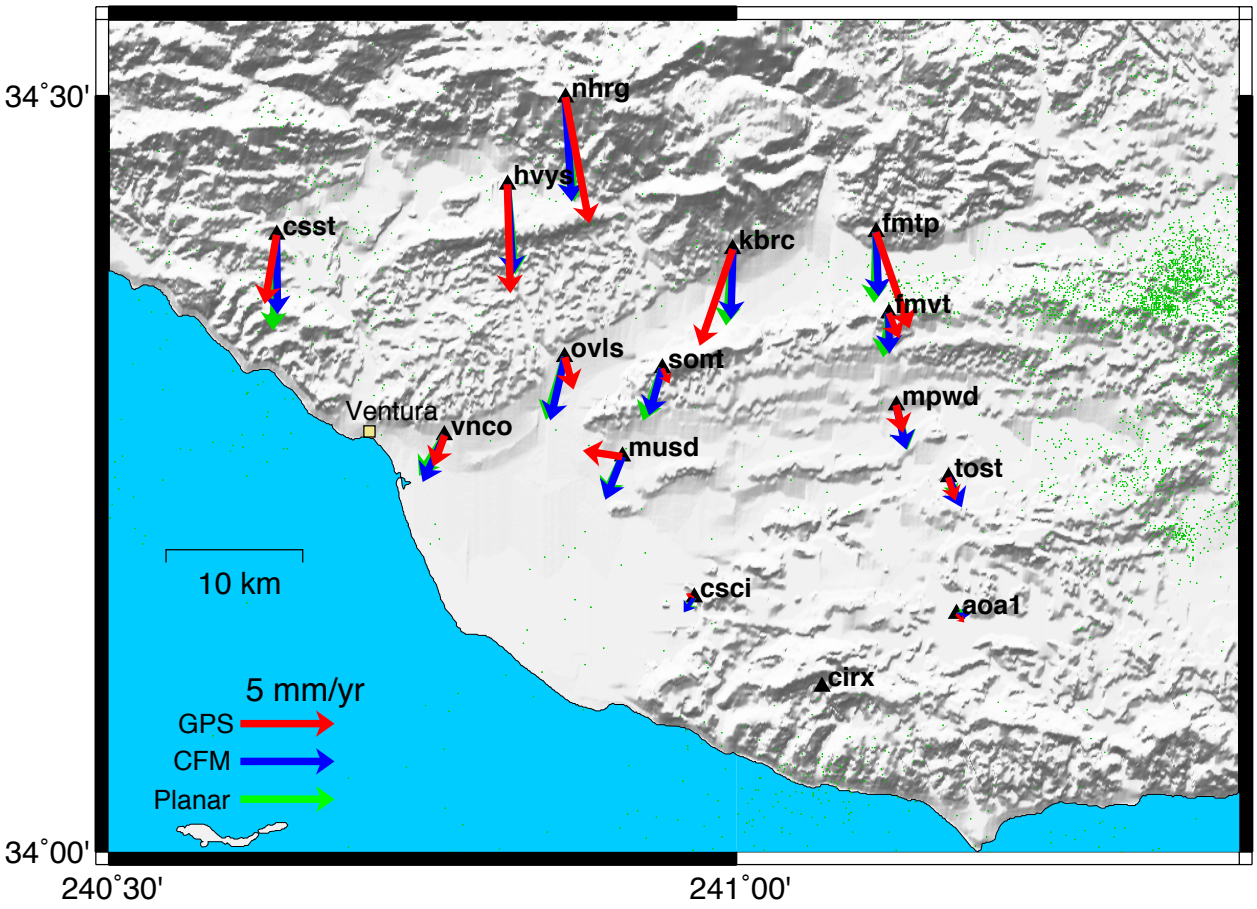

Figure 6: Interseismic GPS and model velocities with 5km locking depth

representation of the geologic faults in this area of the basin. However, the westward movement of station MUSD is particularly enigmatic. The largest discrepancies in velocity rates occur at stations FMTP, SONT and KBRC; the model under-predicts convergence across the eastern portion of the Ventura basin. Inclusion of a compliant basin fill, which promotes localized convergence could partly remedy these rate discrepancies. Changing local fault configuration to more optimally oriented dips may also increase local convergence rates.

3.2 Effects of planar fault surfaces on interseismic surface velocities

The three-dimensional interseismic model with planar faults produces similar surface velocities to the model with geologically more accurate non-planar fault surfaces (Fig. 6). Noticeable differences arise in the eastern Ventura basin and at station CSST. These differences are not great enough to distinguish planar or non-planar fault geometry from the interseismic surface velocity pattern. Because the changes in the interseismic fault geometry occur below the locking depth, the effect of these changes on the surface are muted. The small differences observed may be due to differences in slip interaction between faults that arise when geometry is altered. Although the distinction between interseismic surface velocities of planar and non-planar faults is small, the differences in slip interaction and distribution may be significant for estimating seismic hazard.

4. Slip rates

Both the GPS and model predict some station velocities that are oblique to the trend of fault that bound the Ventura basin (e.g. station KBRC). This obliquely implies significant strike-slip along the major basin bounding faults. These models may provide the most reliable estimate of strike on these faults because paleoseismic investigators in the area have not been able to document such slip. Furthermore, strike slip on these faults is neglected by previous two-dimensional analyses of the region.

We first compare modeled fault slip vector rake and slip rates to ranges calculated from past geologic and paleoseismic studies. Since our models contain fault surfaces with many hundreds of elements we present average slip vector rake and slip rates and weighted by element size.

4.1 Effects of planar fault surfaces on slip sense and slip rates

All of the modeled Ventura region faults have a non-zero strike-slip component, including the basin-bounding San Cayetano, Red Mountain, and Oak Ridge faults (Fig. 7a). In the non-planar topology model we observe that Simi / Santa Rosa, and Sisar are the only faults that have rakes within ~10^{o} of being pure dip-slip. As is intuitively expected, most of the planar surfaces exhibit a larger component of oblique slip than non-planar fault surface because along strike topology resists strike-slip motions. Malibu Coast and Santa Ynez faults both exhibit oblique right-lateral reverse slip, whereas past studies suggest left-reverse separation across these faults. This discrepancy warrants further investigation into the slip sense and fault geometry of these faults.

As with interseismic surface velocity, we observe that the planar fault model predicts slip rates that are quite similar to the complex topology model and vary by a maximum of ~1.5 mm/yr (e.g. Santa Susana; Fig. 7b). Because planar faults have

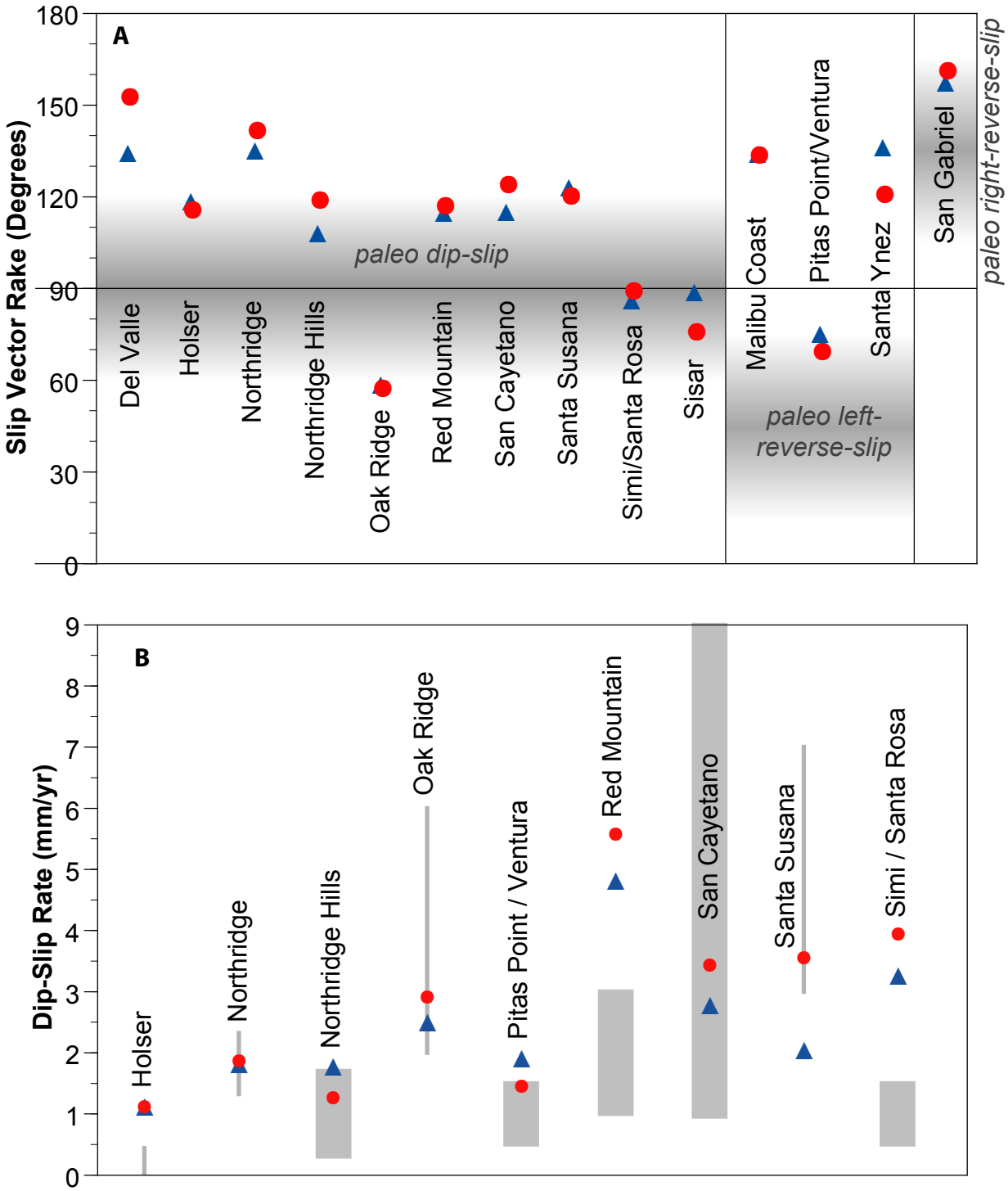

Figure 7: A) The slip vector rakes of modeled surfaces. We use a right-hand convention, where slip rake is measured from 0˚ for pure right-lateral strike-slip faulting to 180˚ for pure left-lateral strike slip faulting. Pure reverse-slip faults have a slip vector of 90˚. Faults are grouped according to their geologically observed slip sense, with primarily reverse-slip faults on the left. Results from the topology model are shown in blue triangles while results from the planar model are shown with red circles. The shaded boxes represent approximate accepted ranges for each group of faults based on past studies. B) Dip slip rates from the topology model are represented as triangles and the planar model results are shown as circles. Grey bars indicate the expected range of dip-slip rates from paleo-seismic studies (thick) and 2D balanced cross section analysis (thin).

fewer asperities to resist slip, the planar model typically produces faster slip rates. The exception is the Pitas Point / Ventura fault, which when simplified into a planar surface has a slower slip rate. This is because, the CFM version of the Pitas Point / Ventura fault has a concave to the south surface trace and a steep dip, and when an average strike and dip are calculated, the resultant plane has a strike azimuth of ~265° and a dip of ~76°. The resultant plane, while oriented approximately perpendicular to the contraction direction, is very steep and therefore not optimally oriented to accumulate reverse slip.

Most faults in the Ventura basin are slipping at rates close to the geologic slip rates constrained by previous studies (Fig. 7b). Exceptions include the non-planar Santa Susana fault, which slips slower than previous estimates, and the Holser, Red Mountain and Simi/Santa Rose faults, which slip faster than previous estimates. The discrepancies between the model and paleoseismic/geology rates may be due in part to inaccurate fault geometry or inaccurate geologic slip estimates. For example, if, rather than extending the Simi fault to a depth of 27.5 km to the moho, we abutted the Simi fault against the intersecting Oak Ridge fault, dip slip rates along the smaller Simi fault would slow significantly. Inaccurate geologic slip estimates may arise from kinematic analysis of two-dimensional cross-sections, which both ignore deformation out of the plane of section and often overlook deformation within rock between faults.

Another large slip rate discrepancy occurs along the Red Mountain fault, which is slipping faster than 5 mm/yr in the non-planar model and > 6 mm/yr in the planar model. These rates approximately double the past rate estimates along the Red Mountain fault. While past studies have based slip rates estimates on studies in the onshore portions of the fault trace, the Red Mountain fault extends offshore for ten's of km. The onshore portions of the Red Mountain fault in our topology model are slipping much closer to the 1-3 mm/yr previously estimated rates for this fault (Fig. 8). Fault topology may account for the variation in slip rate along the fault trace. Slip is more uniformly distributed along the planar Red Mountain fault so that the planar model predicts nearly two times faster slip rates in the onshore portions than does the topology model.

4.3 Implications for representative slip rates on faults

To illustrate the difficulty of estimating a representative slip rate from one trench site location, we examine slip rates at four hypothetical trench locations along the Red Mountain fault (Fig. 8). If a slip estimate were calculated in the field at location A, our model predicts ~5 mm/yr net slip with dominant reverse and minor right-lateral slip, while our model predicts ~3 mm/yr at site B with similar slip sense. Site C would yield a nearly pure reverse slip of 6 mm/yr. While correct for their respective locations, only site A matches the 5.32 mm/yr average slip rate with a 2:5 ratio of right-lateral strike-slip to dip slip of the modeled Red Mountain fault (Table 2).

These maps can be used to either choose representative slip locations along the fault for paleoseismic investigation. Alternatively, assuming that model calculated slip distributions are accurate, paleoseismic analysis at any of these sites could be scaled or corrected to yield a slip rate which is representative of the entire fault surface.

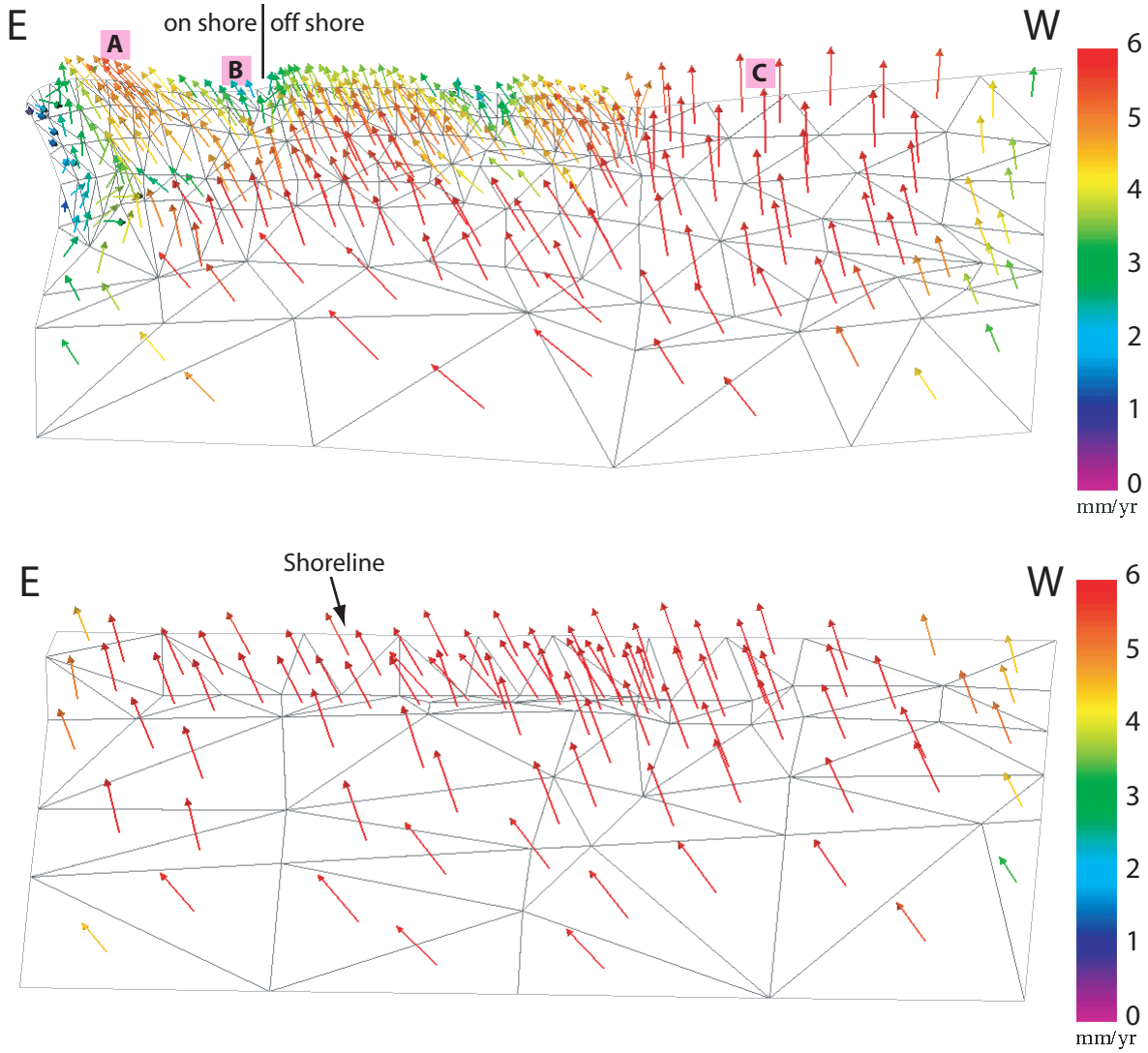

Figure 8 – Slip distribution on the modeled Red Mountain fault surface (viewing to the South). Comparison of the planar and non-planar slip distribution revelas that the planar fault surface representation overestimates the near surface slip in near the surface and on-shore by more than a factor of two. Past slip rates have been based on onshore studies, which match better the slip rates from the non-planar model. Additionally, the past studies have been conducted in areas where the fault is slipping at much lower rates than are representative of average values for the Red Mountain fault. LocationsA, B and C show hypothetical trench locations that do not nessecarily reveal slip direction and slip rate information representative of the Red Mountain fault.

5 Conclusions

The three-dimensional models demonstrate that considerable strike slip along faults within the Ventura basin is neglected in two-dimensional studies. Consequently, two-dimensional analyses of the Ventura basin ignore a significant portion of the net slip along the fault surface and lead to undercharacterization of seismic hazard. The three-dimensional interseismic model results match well the pattern of geodetic surface velocities but with a geologically unreasonably shallow locking depth. Compliant sedimentary basin fill is needed to match reasonable seismogenic locking depths in the interseismic model.

Three-dimensional interseismic models with planar and non-planar fault surfaces below the seismogenic locking depth within the Ventura basin show little difference in surface velocity pattern. Thus, interseismic surface velocities cannot resolve between planar and non-planar fault topology within the Ventura basin. The distribution of slip, however, is sensitive to fault topology. The variation of slip along fault surfaces demonstrates that many sites would not yield representative slip rates values nor, in some cases, accurate overall slip sense. Fault slip distributions produced by three-dimensional models should be considered when estimating representative slip rates from paleoseismic investigations.

6. References

Aoki, Y., and C.H. Scholz, Vertical deformation of the Japanese islands, 1996-1999, *Journal of Geophysical Research, B, Solid Earth and Planets*, *108* (B5), 2003.

Austin, K., and S. Owen, Use of a Principal Component Analysis to Analyze GPS Time Series from the Ventura Basin and Hector Mine Region, SCEC Annual Meeting, September 2004

Azor, A., et al. (2002), Geomorphic indicators of active fold growth; South Mountain-Oak Ridge Anticline, Ventura Basin, Southern California, Geological Society of America Bulletin, 114, 745-753.

Bawden, G., et al. (2001), Tectonic contraction across Los Angeles after removal of groundwater pumping effects, Nature, 412, 812-815.

Budiansky, and O'Connell (1974), Seismic velocities in dry and saturated cracked solids, Journal of Geophysical Research, 79, 5412-5426.

Cemen, I. (1979), Structure of San Cayetano and Oak Ridge thrust faults, East-central Ventura Basin, California, AAPG Bulletin, 63, 844.

Cooke, M. L., et al. (in preparation), Fault slip rates determined from three-dimensional models of the Los Angeles metropolitan area, California, for Geophysical Research Letters.

Dolan, J. F., and T. Rockwell (2001), Paleoseismic evidence for a very large (M (sub w) >7), post-A D 1660 surface rupture on the eastern San Cayetano Fault, Ventura County, California; was this the elusive source of the damaging 21 December 1812 earthquake?, Bulletin of the Seismological Society of America, 91, 1417-1432.

Donnellan, A., et al. (1993), Geodetic measurement of deformation in the Ventura Basin region, Southern California, Journal of Geophysical Research, 98, 727-721.

Fuis, G. S., et al. (2001), Crustal structure and tectonics from the Los Angeles basin to the Mojave Desert, southern California, Geology, 29, 15-18.

Griffith, W. A., and M. L. Cooke (2004), Mechanical validation of the three-dimensional intersection geometry between the Puente Hills blind-thrust system and the Whittier fault, Los Angeles, California, Bulletin of the Seismological Society of America, 94, 493-505.

Griffith, W. A., and M. L. Cooke (2005), How sensitive are fault slip rates in the Los Angeles Basin to tectonic boundary conditions?, Bulletin of the Seismological Society of America, 95, 1263-1275.

Hager, B. H., et al. (1999), Reconciling rapid strain accumulation with deep seismogenic fault planes in the Ventura Basin, California, Journal of Geophysical Research, 104, 207-225.

Huftile, G. J., and R. S. Yeats (1994), Late Quaternary structure and convergence rates in the coastal Ventura Basin, AAPG Bulletin, 78, 666.

Huftile, G. J., and R. S. Yeats (1995), Convergence rates across a displacement transfer zone in the western Transverse Ranges, Ventura Basin, California, Journal of Geophysical Research, 100, 2043-2067.

Maerten, F., et al. (2005), Inverting for Slip on Three-Dimensional Fault Surfaces Using Angular Dislocations, Bulletin of the Seismological Society of America, 95, 1654–1665.

Muller, J. R., and A. Aydin (2005), Using mechanical modeling to constrain fault geometries proposed for the northern Maramara Sea, Journal of Geophysical Research, 110.

Olson, E. L., and M. L. Cooke (2005), Application of three fault growth criteria to the Puente Hills thrust system, Los Angeles, California, USA, Jounal of Structural Geology, 27, 1765-1777.

Plesch, A., et al. (2002), SCEC 3D community fault model for southern California, paper presented at Fall Meeting of the American Geophysical Union, San Francisco, CA.

Rockwell, T. K. (1988), Neotectonics of the San Cayetano Fault, Transverse Ranges, California, Geological Society of America Bulletin, 100, 500-513.

Savage, J.C., Principal component analysis of interseismic deformation in Southern California, *Journal of Geophysical Research, B, Solid Earth and Planets*, *100* (7), 12,691-12,701, 1995.

Savage, J. C., and R. Burford (1970), Accumulation of tectonic strain in California, Bulletin of the Seismological Society of America, 60, 1877-1896.

Savage, J.C., and W. Thatcher, Interseismic deformation at the Nankai Trough, Japan, subduction zone, *Journal of Geophysical Research, B, Solid Earth and Planets*, *97* (7), 11,117-11,135, 1992.

Shen, Z.-K., et al. (1996), Crustal deformation across and beyond the Los Angeles Basin from geodetic measurements, Journal of Geophysical Research, B, Solid Earth and Planets, 101, 27,957-927,980.

Thomas, A. L. (1994), POLY3D: A Three-Dimensional, Polygonal Element, Displacement Discontinuity Boundary Element Computer Program with Applications to Fractures, Faults, and Cavities in the Earth's Crust, Master's thesis, 52 pp, Stanford University.

Wdowinski, S., Y. Bock, J. Zhang, P. Fang, and J. Genrich, Southern California Permanent GPS Geodetic Array; spatial filtering of daily positions for estimating coseismic and postseismic displacements induced by the 1992 Landers earthquake, *Journal of Geophysical Research, B, Solid Earth and Planets*, *102* (8), 18,057-18,070, 1997.

Yeats, R. S. (1988), Late Quaternary slip rate on the Oak Ridge Fault, Transverse Ranges, California; implications for seismic risk, Journal of Geophysical Research, 93, 137-112.

Table 1. Average time series RMS

	Unfiltered	Common Mode Filter	Common Mode & PCA Filter
East (mm)	3	0.8	0.3
North (mm)	2	0.7	0.2
Vertical (mm)	6	3	0.7

Table 2 Model-calculated slip rates and differences

	Net Slip (mm/yr)			***Dip-Slip (mm/yr)***			***Strike-Slip (mm/yr)***			***Strike-Slip Ratio***		
Fault Name	***Topology***	***Planar***	***Difference***	***Topology***	***Planar***	***Difference***	***Topology***	***Planar***	***Difference***	***Topology***	***Planar***	***Difference***
Del Valle	0.62	1.23	*0.62*	0.44	-0.58	*-1.02*	-0.43	-1.09	*0.66*	0.99	1.89	*0.90*
Holser	1.29	1.25	*-0.04*	1.13	1.13	*0.00*	-0.62	-0.53	*-0.09*	0.55	0.47	*-0.08*
Malibu Coast	2.86	2.79	*-0.06*	2.05	2.03	*-0.01*	-1.99	-1.91	*-0.08*	0.97	0.94	*-0.03*
Northridge	2.60	3.01	*0.41*	1.83	1.88	*0.05*	-1.84	-2.34	*0.50*	1.01	1.24	*0.24*
Northridge Hills	1.87	1.46	*-0.42*	1.78	1.28	*-0.50*	-0.59	-0.70	*0.11*	0.33	0.54	*0.21*
OakRidge	2.93	3.50	*0.57*	2.50	2.93	*0.42*	1.52	1.92	*0.40*	0.60	0.65	*0.05*
Pitas Point	1.99	1.57	*-0.41*	1.92	1.47	*-0.45*	0.51	0.56	*0.06*	0.26	0.38	*0.12*
Red Mountain	5.32	6.25	*0.93*	4.82	5.59	*0.77*	-2.25	-2.80	*0.55*	0.47	0.50	*0.03*
San Cayetano	3.08	4.14	*1.06*	2.78	3.45	*0.67*	-1.31	-2.28	*0.97*	0.47	0.66	*0.19*
San Gabriel	6.88	7.33	*0.45*	2.63	2.42	*-0.21*	-6.36	-6.92	*0.56*	2.42	2.86	*0.44*
Santa Susana	2.46	4.10	*1.65*	2.05	3.56	*1.51*	-1.35	-2.03	*0.69*	0.66	0.57	*-0.09*
Santa Ynez	2.72	2.63	*-0.10*	1.88	2.26	*0.38*	-1.97	-1.33	*-0.64*	1.05	0.59	*-0.46*
Simi/Santa Rosa	3.28	3.96	*0.68*	3.27	3.96	*0.69*	0.21	0.09	*-0.12*	0.07	0.02	*-0.04*
Sisar	0.60	1.78	*1.18*	0.60	1.72	*1.12*	0.01	0.45	*0.44*	0.02	0.26	*0.25*